Ionics (2006) 12: 21–32
DOI 10.1007/s11581-006-0007-5

ORIGINAL PAPER

C. M. Julien · A. Ait-Salah · A. Mauger · F. Gendron

Magnetic properties of lithium intercalation compounds

Received: 13 December 2005 / Accepted: 25 January 2006 / Published online: 26 April 2006

Abstract Magnetic experiments are powerful tools to study fundamental properties and to check the qualities of samples. Temperature, stress, and impurities of materials can all affect magnetic properties and play an important role in the utilization of these materials for engineering applications. The estimation and analysis of the spontaneous magnetization can reveal ferromagnetic particles as impurities in samples. The shape of the temperature dependence of magnetization is indicative of the origin of the magnetic properties. However, it is necessary to correlate the $\chi_m(T)$ curves and isothermal $M(H)$ plots to achieve a complete analysis of the electronic properties of the materials. Highlights of magnetic properties of lithium intercalation compounds are briefly described. Intrinsic and extrinsic properties are considered as useful parameters to determine the purity of electrode materials for rechargeable Li-ion batteries.

Keywords Li-ion batteries · Intercalation compounds · Magnetic properties · Clustering

Introduction

Magnetism continues to be an important subject, both to provide insights into the understanding of condensed matter and cooperative phenomena and for the development of technologically important materials and devices. Materials may be classified into five categories by their responses to externally applied magnetic fields, i.e., dia-, para-, ferro-, ferri-, and antiferromagnetic substances. The study of magnetic properties in the solid state implies an examination of the interaction between the electrons associated with the metal ions, which are substance-specific. Consequently, these magnetic properties differ greatly in strength. Diamagnetism is a property of all materials and opposes applied magnetic fields, but it is a very weak phenomenon. Paramagnetism, when present in semiconductors, can be stronger than diamagnetism and produces magnetization in the direction of the applied field, and proportional to the applied field. Ferromagnetic and ferrimagnetic effects are very large: They produce magnetizations sometimes orders of magnitude larger than the applied field and, as such, are much larger than either diamagnetic or paramagnetic effects.

Magnetic measurements can be extended to study magnetic structure and electronic properties of materials used in lithium power sources, i.e., the so-called lithium intercalation compounds (LiICs). Because Li ions are nonmagnetic (diamagnetic), they indirectly affect magnetic properties through influence on the cation valence of the 3d iron-transition element. Magnetic properties are determined by the structure of sublattice in the oxide framework, the nature of the metal ions, and the electronic states. In this context, magnetic properties are of particular interest because they are found to be a powerful tool to characterize materials, in particular, when impurities and nanoparticles cannot be detected by classical analysis, i.e., X-ray diffraction (XRD), Fourier transform infrared (FTIR) spectroscopy, etc. Magnetism is therefore indirectly important to the electrochemical properties of materials as well.

Magnetic measurements are also tools used to check the quality of samples. The estimation and analysis of the spontaneous magnetization can reveal the existence of ferromagnetic (ferrimagnetic) particles in samples. The shape of the temperature dependence of magnetization $M(H)$ is indicative of the origin of the magnetic properties. However, it is necessary to correlate the magnetic susceptibility $\chi_m(T)$ curves and isothermal $M(H)$ plots for a

C. M. Julien (✉) · A. Ait-Salah · F. Gendron
Institut des Nano-Sciences de Paris (INSP),
Université Pierre et Marie Curie,
CNRS-UMR 7588,
Campus Boucicaut, 140 rue de Lourmel,
75015 Paris, France
e-mail: christian.julien@insp.jussieu.fr

A. Mauger
Department MIPPU, CNRS,
Campus Boucicaut, 140 rue de Lourmel,
75015 Paris, France

complete analysis of the electronic properties of materials [1].

One goal of the work carried out in our laboratory is the understanding of the local structure in LiICs using resonance spectroscopy, i.e., Raman scattering, Fourier transform infrared, electron spin resonance, and magnetic measurements. This paper presents the magnetic properties of some LiICs to correlate the structural and electronic properties of oxides used as positive electrode materials in rechargeable lithium-ion batteries. Here, we consider typical materials such as compounds of the α-$NaFeO_2$-type structure, i.e., $LiNiO_2$ and $LiFeO_2$; Li–Mn–O frameworks with the spinel structure, i.e., $LiMn_2O_4$ and $LiCoMnO_4$; and the phospho-olivine lattices, i.e., $LiFePO_4$, $LiMnPO_4$, and $LiNiPO_4$. The characterization of the magnetic nanoparticles incorporated in these frameworks is deduced from the magnetic susceptibility and magnetization measurements.

Experimental procedure

Nowadays, most of the magnetic properties are studied by various techniques such as neutron diffractometry, magnetometry, NMR, and electron spin resonance. The two resonance spectroscopies are also useful tools for characterizing the local structure in materials.

The microscopic magnetic structure of materials is most often studied by using neutron scattering techniques, and experiments are performed to measure the structure and excitation for all classes of magnetic materials. More recently, synchrotron sources have been used to study the magnetic scattering. The range of wavelength and energy possessed by thermal moderated neutrons allows us to study not only the nuclear long-range, static nature of solids, but also the dynamics (phonons). Similarly, the neutron's magnetic moment (S=1/2) can be used as a probe to study the magnetism in solids, allowing unparalleled scrutiny of both the magnetic structures (short- and long-range) and the excitations (magnons) of magnetic materials. Neutron scattering techniques are presently considered as the most powerful probe of magnetic materials. When a material has ferromagnetic ordering, the magnetic lattice is the same as the atom lattice, and no new "Bragg reflections" are created (the intensities of existing Bragg reflections change). For an antiferromagnetic state, however, the magnetic lattice is not the same as the atom lattice, and new, purely magnetic Bragg reflections occur. From the pattern of the magnetic Bragg reflections, the details of the antiferromagnetic ordering structure can be deduced, in the same way that crystal structures are solved from the pattern of the (nonmagnetic) Bragg peaks in XRD and (nuclear) neutron diffraction. Neutron diffraction patterns are currently analyzed using the Rietveld fitting procedure [2].

The use of superconducting quantum interference devices (SQUID) in ultrasensitive magnetic measurement systems may nowadays be considered as a standard technique, to the extent that several companies offer reliable and automated commercial SQUID magnetometers. The SQUID consists of two superconductors separated by thin insulating layers to form two parallel Josephson junctions. The device uses a liquid-helium-cooled amplifier to measure the magnetic moment in the range from 10^{-7} to 300 emu. The field range is from −5.5 to +5.5 T [3].

Data on the temperature dependence of susceptibility are currently recorded on heating the sample using two modes to determine the magnetic behavior: zero-field cooling (ZFC) and field-cooling (FC). The procedure is based on performing two consecutive magnetization measurements: In ZFC, the sample is first cooled down in the absence of a magnetic field and then measured in an applied magnetic field at increasing temperature, FC is performed in a similar magnetic field at decreasing temperature. The results obtained in this way can exhibit a strong dependence of magnetization. The temperature range in which a magnetic hysteresis appears and the temperature at which a magnetic ordering can be detected should be emphasized.

Magnetic properties of solid-state materials

This section summarizes the general trends of magnetic properties for solid-state materials. In electrical engineering, the magnetic susceptibility is the degree of magneti-

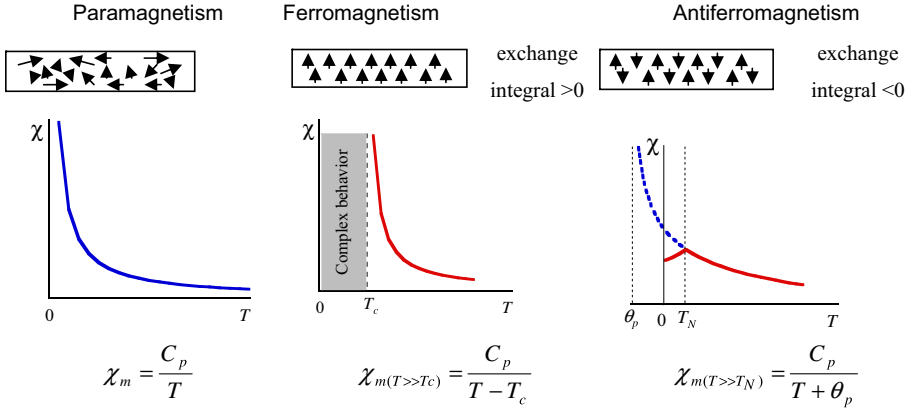

Fig. 1 Temperature dependence of the magnetic susceptibility of paramagnetic, ferromagnetic, and antiferromagnetic solids

Table 1 Electron configurations and net spins for transition element cations and effective magneton numbers for iron group ions [5]

Ion	Configuration	Basic level	Free cation		Cubic field	
			S	p_{eff}	S	p_{eff}
Mn^{4+}, Cr^{3+}	$3d^3$	$^4F_{3/2}$	3/2	3.87	3/2	3.87
Mn^{3+}, Cr^{2+}	$3d^4$	$^5D_0$	2	4.90	1	2.83
Fe^{3+}, Mn^{2+}	$3d^5$	$^6S_{5/2}$	5/2	5.92	1/2	1.73
Fe^{2+}, Co^{3+}	$3d^6$	$^5D_4$	2	4.90	0	0
Co^{2+}, Ni^{3+}	$3d^7$	$^4F_{9/2}$	3/2	3.87	1/2	1.73
Ni^{2+}	$3d^8$	$^3F_4$	1	2.83	1	2.83
Cu^{2+}	$3d^9$	$^2D_{5/2}$	1/2	1.73	1/2	1.73

The free ions and cations in strong cubic fields are considered

zation of a material, M is the magnetic dipole moment per unit volume in response to a magnetic field H, as

$$\chi_m = \frac{\partial M}{\partial H}. \tag{1}$$

If χ_m is positive, the material is called paramagnetic and the magnetic field is strengthened by the presence of the material. If χ_m is negative, then the material is diamagnetic and the magnetic field is weakened in the presence of the material. Figure 1 displays the temperature dependence of the magnetic susceptibility of paramagnetic, ferromagnetic, and antiferromagnetic solids [4].

Paramagnetic materials attract and repel like normal magnets when subjected to a magnetic field. For thermal equilibrium, the magnetization of paramagnets is treated using the Brillouin formalism. Under relatively low magnetic field saturation when the majority of atomic dipoles are not aligned with the field, paramagnetic materials exhibit magnetization according to the well-known Curie–Weiss law, which treats the interaction between spins and molecular field

$$\chi_m = \frac{C_{\text{p}}}{T + \theta_{\text{p}}}, \tag{2}$$

where C_{p} is the Curie constant. The Weiss constant, θ_{p}, typically accounts for magnetic ordering of the electronic moments below the Curie or Néel temperature for uncorrelated spins (in salts, for instance) θ_{p}=0 (see Fig. 1). For a paramagnet having an effective moment μ_{eff}, the Curie constant is written as

$$C_{\text{p}} = \frac{N_A p_{\text{eff}}^2 \mu_{\text{B}}^2}{3k_{\text{B}}}, \tag{3}$$

where N_A is the molar concentration of ions and μ_{B} the Bohr magneton (μ_{B}=9.274×10^{-24} J/T). The effective momentum number p_{eff} is defined as

$$p_{\text{eff}}^{\text{theor}} = 2[S(S+1)]^{1/2}, \tag{4}$$

where S refers to the electronic spin quantum number. Equation (4) is used in the case of the "quenching" of the orbital angular momentum (L=0 and J=S), which occurs frequently for transition-metal ions from the iron group. Table 1 shows the theoretical magneton numbers for iron group ions. Paramagnetic ions with electronic spin, S (e.g., S=3/2 for d^3 ions Mn^{4+} and Cr^{4+}), are associated with magnetic moments, μ_{eff}=−$g\mu_{\text{B}}S$, that align in the presence of static magnetic field H_0.

When the Curie constant is determined experimentally by fitting the linear $\chi_m^{-1}(T)$ curve in the paramagnetic domain, one can estimate the experimental value for p_{eff} and then know the electronic configuration of the magnetic ion (in the quenched configuration) using the following equation:

$$p_{\text{eff}}^{\text{exp}} = \left(\frac{3k_{\text{B}}C_{\text{p}}}{N_{\text{A}}\mu_{\text{B}}^2}\right)^{1/2} = 2.84\sqrt{C_{\text{p}}}. \tag{5}$$

An important class of magnetic materials is that of ferromagnets: iron, nickel, cobalt, and manganese. A ferromagnetic substance possesses a spontaneous magnetic moment even in the absence of an applied magnetic field.

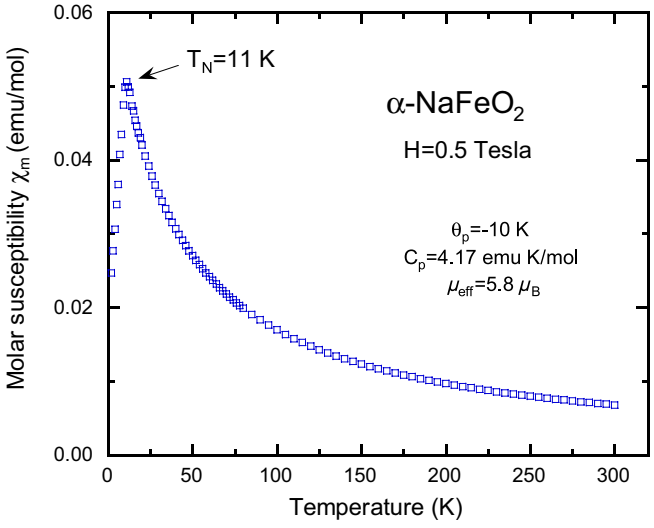

Fig. 2 Temperature dependence of the magnetic susceptibility of α-$NaFeO_2$

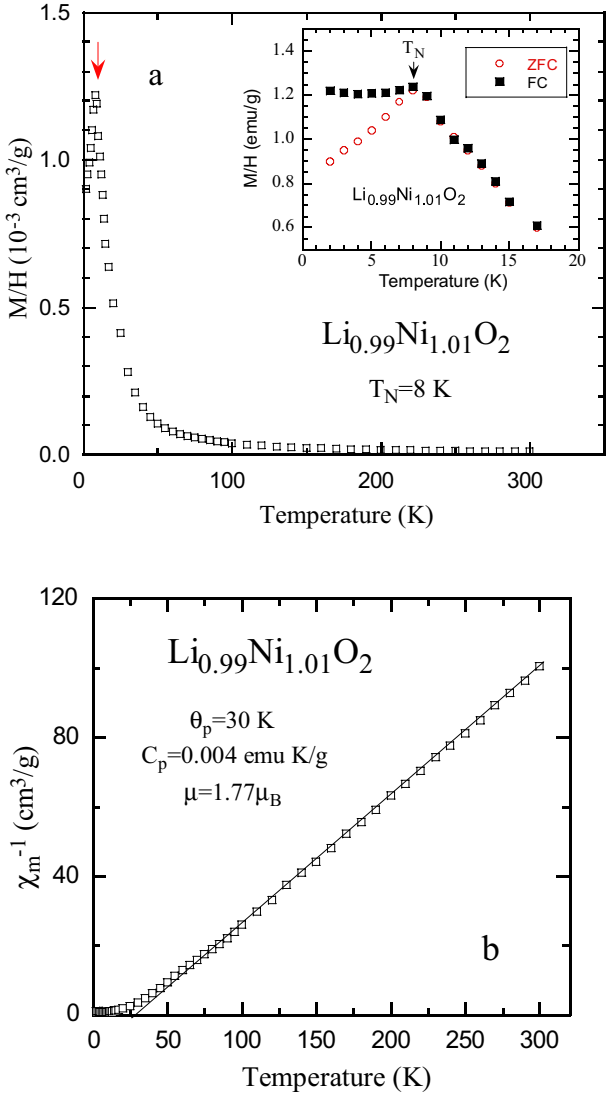

Fig. 3 **a** Temperature dependence of the magnetic susceptibility of $Li_{0.99}Ni_{1.01}O_2$. Insert shows the ZFC and FC low-temperature region. **b** Reciprocal susceptibility of $Li_{0.99}Ni_{1.01}O_2$

The saturation magnetization M_S is defined as the spontaneous magnetic moment per unit volume. The Curie point *Tc* is the temperature above which the spontaneous moment vanishes. For iron, *Tc*=1,043 K [4].

The antiferromagnetic state is characterized by an ordered, antiparallel arrangement of electron spins. The simplest situation in antiferromagnetism arises when the lattice of paramagnetic ions can be divided into two interpenetrating sublattices. We recognize antiferromagnetism by a well-defined kink in the curve of the magnetic susceptibility vs temperature. This kink determines the Néel temperature, T_N. Antiferromagnets are also characterized by a negative value of the Curie temperature. Figure 1 summarizes the temperature dependence of the magnetic susceptibility for paramagnetic, ferromagnetic, and antiferromagnetic solids.

The paramagnetic temperature θ_p (also called the Weiss constant) is defined as the intercept of the temperature-axis of the high-temperature asymptote to the $\chi_m^{-1}(T)$ curve. Depending on the type of antiferromagnetic interactions, θ_p could be positive or negative. It should be emphasized that θ_p is different than the Néel temperature, T_N, which is the temperature at which an antiferromagnetic material becomes paramagnetic—that is, the thermal energy becomes large enough to upset the magnetic ordering within the material. T_N corresponds to the cusp in the $\chi_m^{-1}(T)$ curve.

In metals, the conduction electrons are not spatially localized like electrons in partially filled ionic shells. Thus, the magnetic susceptibility of metals follows the Pauli-type paramagnetism, which is essentially independent on temperature [4]. In contrast, the magnetic susceptibility of localized electrons closely follows inverse temperature dependence due to the thermal agitation of spin moments. The magnetic molar susceptibility of localized moments will exhibit Curie–Weiss behaviors in the absence of strong ferromagnetic, ferrimagnetic, or antiferromagnetic couplings.

Many battery-grade materials are paramagnetic in the discharged or charged state. For example, the positive electrode material $LiMn_2O_4$ is a mixed-valence compound containing Mn^{3+} (d^4) and Mn^{4+} (d^3) ions. Although the low-spin (d^6) Co^{3+} ions (nominally diamagnetic) in $LiCoO_2$ have paired d-electrons in the fully discharged state, $Li_{1-x}CoO_2$ contains Co^{4+} (d^5) ions when charged. $LiNiO_2$ contains the paramagnetic S=1/2 ions Ni^{3+} (d^7) in the discharged state.

Magnetic properties of layered oxides

A wide variety of LiICs have been studied which include layered compounds based on the α-$NaFeO_2$-type structure (e.g., $LiCoO_2$, $LiNiO_2$, $LiNi_{0.5}Mn_{0.5}O_2$). The structure–magnetic relationships of sodium and lithium ferrites have been investigated to evaluate detectable ferromagnetic impurities [6, 7]. The α-$NaFeO_2$-type structure is built by alternating layers of trigonally distorted FeO_6 and NaO_6

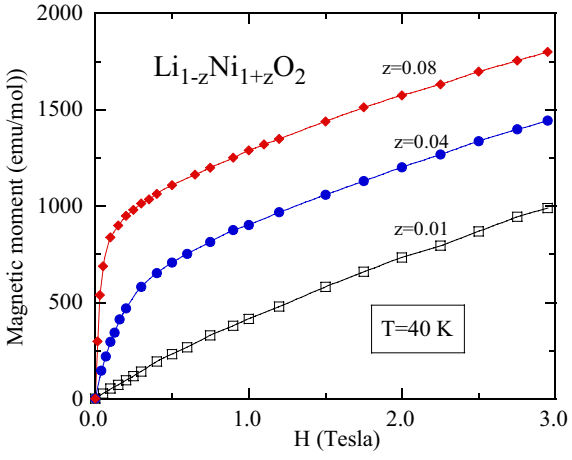

Fig. 4 Magnetization $M(H)$ recorded at 40 K vs stoichiometric deviation in $Li_{1-z}Ni_{1+z}O_2$ layered compound

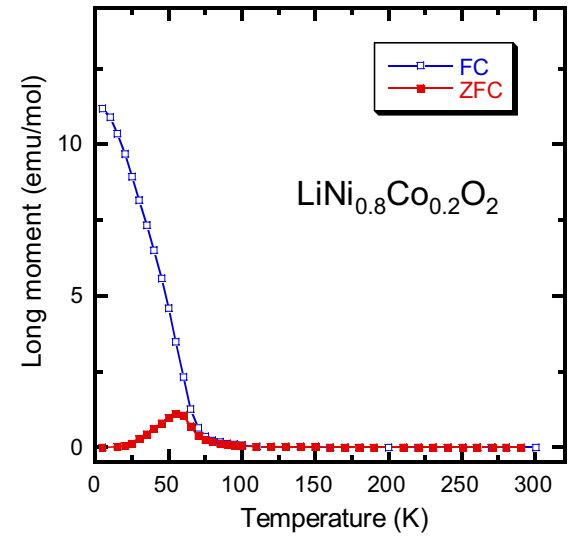

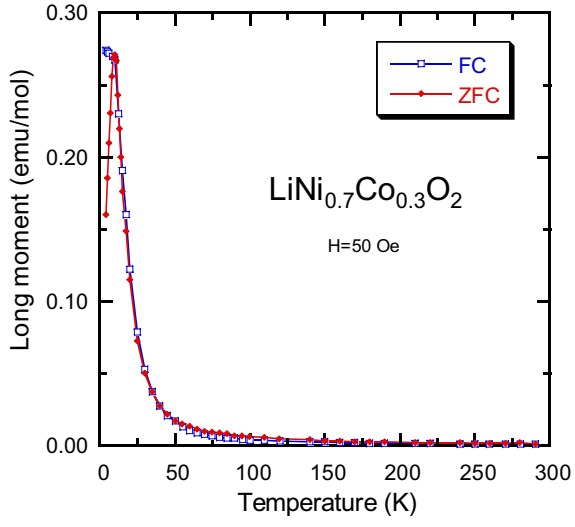

Fig. 5 Temperature of the ZFC and FC molar magnetic susceptibility measured under a field H=50 Oe of $LiNi_{1-y}Co_yO_2$ samples for **a** y=0.2 and **b** y=0.3. A strong deviation from the paramagnetic behavior is observed at low-temperatures for the y=0.2 sample

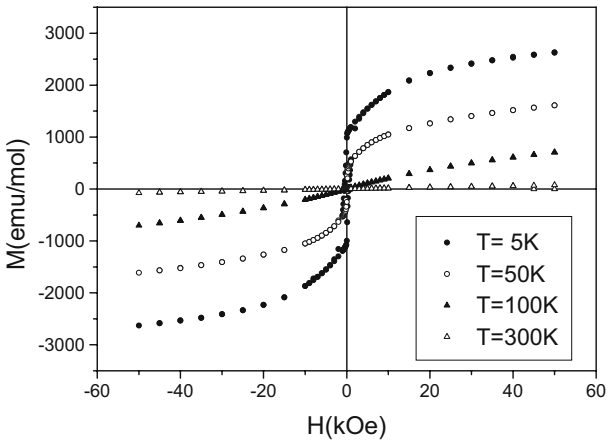

Fig. 6 ZFC magnetization vs applied magnetic field at T=5, 50, 100, and 300 K for $LiNi_{0.8}Co_{0.2}O_2$

octahedra sharing edges. Many $LiMO_2$ (M=Ni, Co, Fe, and Cr) compounds have this typical structure which is suitable for very efficient electrochemical lithium extraction–insertion process. The unit cell is rhombohedral ($R\bar{3}m$ space group). The transition-metal ions M are located in octahedral *3a* (000) sites, and oxygen anions are in a cubic close-packing, occupying the *6c* (00z, 00z) sites. Li cations reside at Wyckoff *3b* (001/2) sites. The transition metal and lithium ions are occupying the alternating (111) planes.

α-$NaFeO_2$

Samples of α-$NaFeO_2$ prepared by hydrothermal treatment of a mixture of α-FeOOH and concentrated NaOH aqueous solution appear as simple antiferromagnets below the Néel temperature T_N=11 K. Therefore, they do not include any ferromagnetic clusters such as Fe_3O_4 or γ-Fe_2O_3 particles. The temperature dependence of the molar magnetic susceptibility is shown in Fig. 2.

Fitting with the Curie–Weiss law, one obtains C_p=4.17 emu K/mol and θ_p=−10 K. The negative θ_p value suggests that antiferromagnetic interactions are present in α-$NaFeO_2$. Using Eq. (2), the effective magnetic moment, μ_{eff}, is calculated to be 5.8 μ_B, which is very close to a spin-only value of high-spin Fe^{3+} (5.92 μ_B).

The effective magnetic moment of $LiFeO_2$ is affected markedly by the contribution of ferromagnetic impurities, easily saturated at the magnetic fields used in the experiments. Two anomalies have been revealed at 40–50 and 90–280 K. The presence of a ferromagnetic impurity such as $LiFe_5O_8$ spinel gives a relatively high μ_{eff} value. The variation of the Néel temperature for various $LiFeO_2$ polymorphs is related to the degree of tetragonal distortion [8].

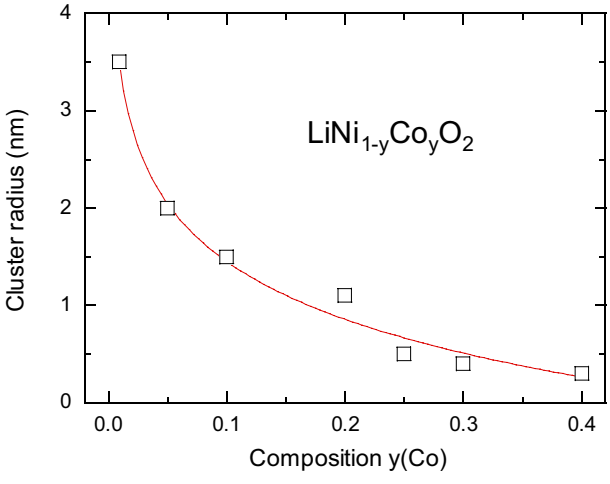

Fig. 7 Size of the ferromagnetic clusters in $LiNi_{1-y}Co_yO_2$ samples

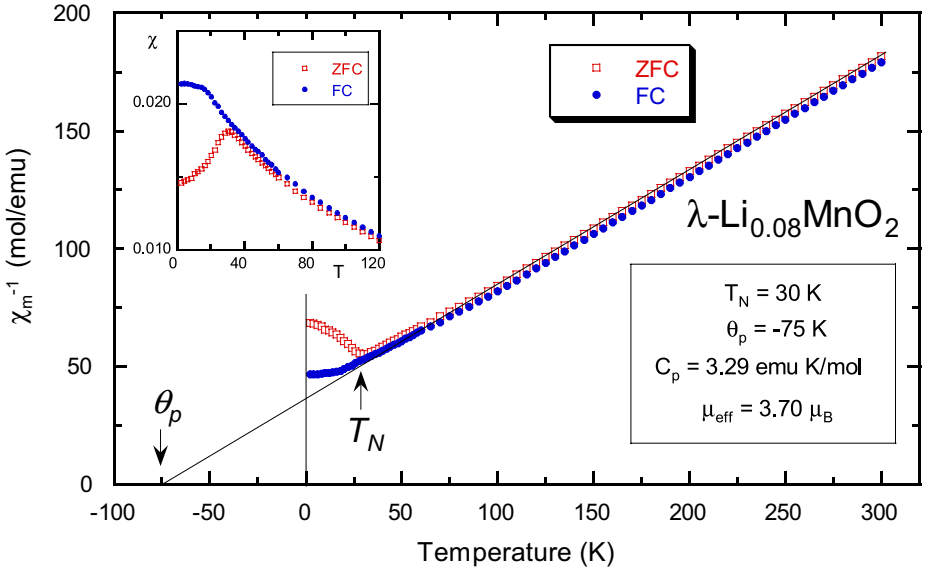

Fig. 8 Inverse ZFC and FC magnetic susceptibility for λ-$Li_{0.08}Mn_2O_4$ as a function of temperature in a field of 0.1 T

$LiNiO_2$

The difficulty of obtaining stoichiometric $LiNiO_2$ free from the presence of excess Ni ions randomly distributed at predominantly Li sites (*3b* Wyckoff position) is known. The magnetic properties are extremely sensitive to the Ni^{2+} ion distribution and should be useful to evaluate the stoichiometry deviation in $Li_{1-x}Ni_{1+x}O_2$. However, the confusion of magnetic properties lies in the quality of the sample. Hirakawa et al. suggested an S=1/2 Ising-type antiferromagnetic triangular lattice in the crystal [9]. Other possibilities, such as ferri-magnetism [10], ferromagnetism [11], a new type of spin-frozen states [12], and spin glass [13–16], have been evoked.

Figure 3a shows the temperature dependence of the magnetic susceptibility of $Li_{0.99}Ni_{1.01}O_2$. The insert displays the ZFC and FC low-temperature region. After ZFC, a cusp-like peak is observed at 8 K corresponding to the Néel temperature. On the other hand, the FC susceptibility shows little temperature dependence below T_N. Such behavior is that of a typical spin glass. The reciprocal susceptibility (Fig. 3b) follows the Curie–Weiss law above 100 K. The parameters obtained by least-square fitting [Eq. (2)] are C_p=0.004 emu K/g and θ_p=30 K. The effective Bohr magneton number is p_{eff}=1.77. This value is close to that of Ni^{3+} ion at low-spin state (S=1/2, p=2[S(S+1)]$^{1/2}$=1.73). The small deviation of the experimental p_{eff} is due to the presence of Ni^{2+} ions (S=1, p=2.83) at the *3b* sites.

Considering that the total susceptibility of a given material is the sum the susceptibility of the various magnetic cations present in the lattice, the effective momentum number p_{eff} of $Li_{0.99}Ni_{1.01}O_2$ is defined as

$$p_{\text{eff}} = \left[(1-z)p^2_{\text{eff}(\text{Ni}^{3+})} + zp^2_{\text{eff}(\text{Ni}^{2+})}\right]^{1/2}, \quad (6)$$

As magnetic measurements are extremely sensitive to the Ni distribution, Eq. (6) is used to evaluate the stoichiometry deviation in $Li_{1-z}Ni_{1+z}O_2$. From Fig. 3, one determines the quantity z=0.01.

Figure 4 shows the applied magnetic field dependence on the magnetization curves $M(H)$ as a function of the stoichiometric deviation, z, in $Li_{1-z}Ni_{1+z}O_2$. The samples were subjected to ZFC down to 4 K and a magnetic field was applied. These data, recorded at 40 K (paramagnetic phase), show clearly the systematic dependence of the effect of stoichiometric deviation on the magnetic behavior. The magnetization can be divided into an extrinsic component of ferromagnetic clusters which saturate easily under the application of a magnetic field of few hundred Gauss, plus the intrinsic part which remains linear in H up to the largest field investigated. Using the superparamag-

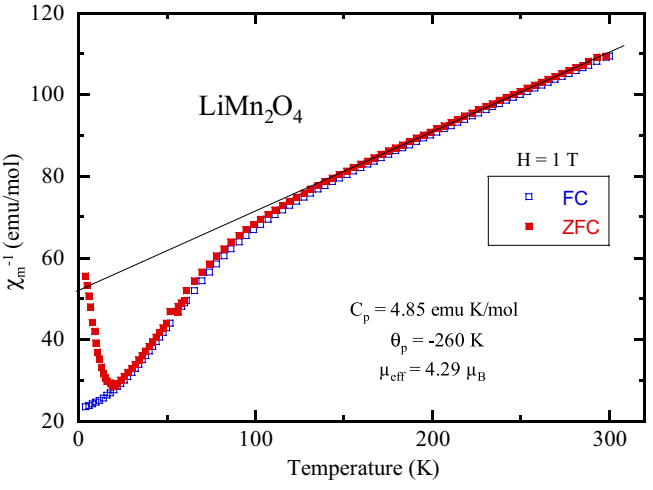

Fig. 9 The reciprocal magnetic susceptibility of $LiMn_2O_4$ sample synthesis by succinic-assisted sol-gel method

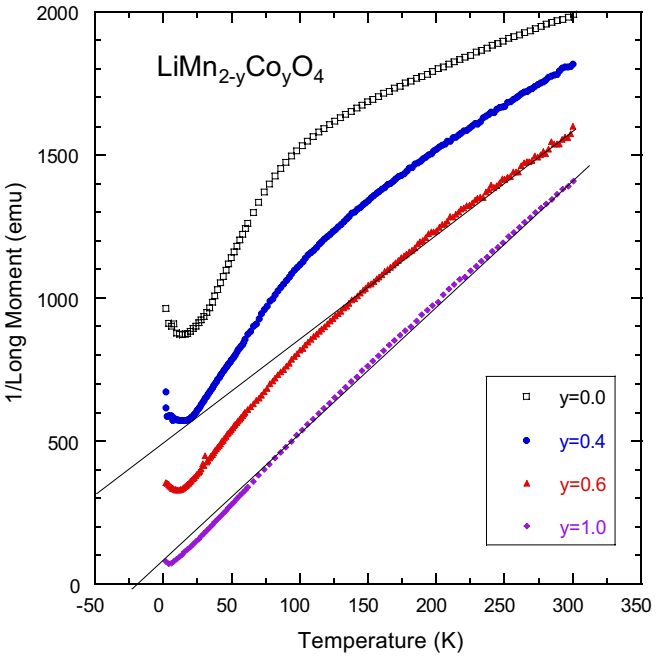

Fig. 10 Temperature dependence of the reciprocal magnetic susceptibility of Co-substituted $LiMn_{2-y}Co_yO_4$ spinels

netic formalism, the magnetization curves are readily computed from the equation:

$$M = M^{\mathrm{clu}} + \chi_{\mathrm{int}} H, \tag{7}$$

where χ_{int} is the intrinsic susceptibility and $M^{\mathrm{clu}}(T,H)$ is the self-consistent solution of Eq. (6)

$$M^{\mathrm{clu}}(T,H) = N\mu_{\mathrm{eff}}(0)\pounds\left(\frac{n\mu_{\mathrm{eff}}(0)H}{k_{\mathrm{B}}T}\right). \tag{8}$$

£ is the Langevin function, N represents cluster concentration, n is the concentration of ferromagnetic particles per cluster, and μ_{eff} is the magnetic moment associated with one cluster. Here the Langevin function can be used due to the presence of macroscopic spins $\mu_{\mathrm{eff}}(0)$. Using Eqs. (7) and (8), the fit of the magnetization curve allows us to determine the Ni^{2+} content in $Li_{1-z}Ni_{1+z}O_2$.

$LiNi_{1y}Co_yO_2$

Because isostructural $LiCoO_2$–$LiNiO_2$ solid solutions display better electrochemical cyclability than parent oxide end-members, it is now generally recognized that $LiNi_{0.8}Co_{0.2}O_2$ is a potential next-generation positive electrode material to replace $LiCoO_2$. $LiNi_{1-y}Co_yO_2$ compounds with $0 \le y \le 1$ were prepared as polycrystalline nanomaterials ($d \approx 200$ nm) following a low-temperature sol-gel method [17]. XRD studies indicate that these materials are single phase for $0.2 \le y \le 1.0$ with an ordered distribution of Li and Ni/Co in the layered structure. Nevertheless, as this technique provides only averaged structural information, it is still possible that, locally, there are some defects, among them disorder, that could affect the electrochemical behaviors of these materials. In fact, through FTIR spectroscopy, we observe for the Li–O band a slight deviation from a linear behavior for high nickel content ($y \le 0.2$), which is attributed to the presence of Ni cations in the octahedral interstices of the predominantly lithium layers (cation mixing). In addition, by means of magnetic measurements, $\chi_m(T)$ and $M(H)$, we detect in all the samples a ferrimagnetic signal, which gets smaller and smaller as the Co content increases, but indeed reveals the presence of some Ni^{2+} ions occupying Li^+ sites that would lead to the formation of small ferromagnetic islands. From those magnetic measurements, we have estimated the size of nanometric magnetic inhomogenities.

Figure 5a and b show the temperature dependence of the magnetic moment of $LiNi_{1-y}Co_yO_2$ for $y=0.2$ and $y=0.3$, respectively. The first general observation is that the samples with high Ni content ($y \le 0.2$) show ferrimagnetic behavior with a value of Tc, which quickly decreases from $Tc_{(y=0)} \sim 215$ K to $Tc_{(y=0..2)} \sim 65$ K as y increases, as seen in the $\chi_m(T)$ and $M(H)$ curves (Fig. 6). Taking into account that perfectly stoichiometric $LiNiO_2$ is considered to be a frustrated antiferromagnetic compound [18], this ferrimagnetic response would be indicative of the existence of Ni^{2+} ions occupying Li^+ places [18, 19]. These interslab ions would lead to a ferromagnetic ordering of the Ni ions in two adjacent $(Ni_{1-y}Co_yO_2)_n$ slabs and to the formation of small ferromagnetic islands in their surroundings with the concomitant apparent ferrimagnetic behavior.

In the samples with intermediate substitutions ($0.2 < y \le 0.4$), the magnetic features are different. Partial substitution of Ni^{3+} by Co^{3+} suppresses the ferrimagnetic response, reflecting that the addition of Co^{3+} inhibits the presence of the interlayer Ni^{2+} ions, and therefore favors a better lamellar structure. The positive Curie–Weiss constant calculated for $100 < T < 300$ K ($\theta_p \approx +30$ K) shows that the Ni–O–Ni nearest neighbor interactions are still present at intermediate substitution levels. Apart from these general trends, magnetic measurements can also provide an approximation to the size of these magnetic islands. In this context, a blocking temperature, which decreases as

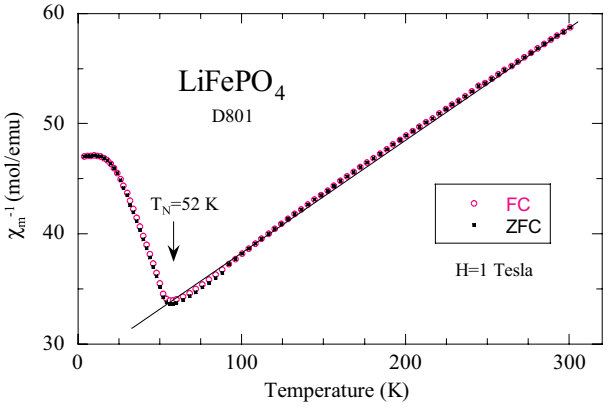

Fig. 11 The temperature dependence of the reciprocal ZFC and FC magnetic susceptibility of $LiFePO_4$ measured at $H=1$ T

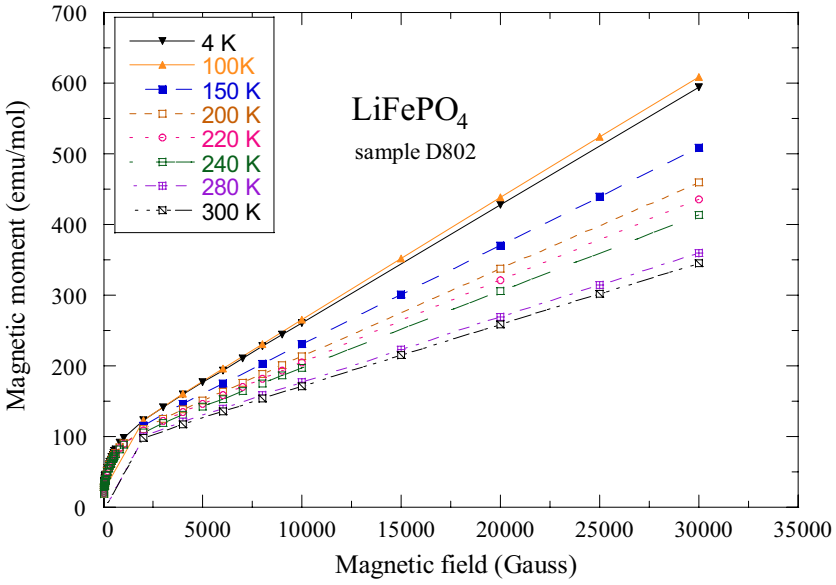

Fig. 12 Magnetization of $LiFePO_4$ as a function of the applied field in the temperature range 4–300 K

the Co content increases, is observed in all the ZFC- and FC-type curves for $\chi_m(T)$. In the high-field region, at this temperature, it is possible to obtain the magnetic anisotropy, K, from the magnetization measurements vs the magnetic field. To do so, we have to take into account that the magnetization approach to saturation can be fitted to the expression [1]

$$M(H) = M_S\left(1 - \frac{a}{H} - \frac{b}{H^2}\right) + cH, \tag{9}$$

where M_S is the saturation magnetization and a, b, and c are suitable constants. The second term, cH, is the low-field contribution, which is negligible near the saturation. Two examples of these fits for the $LiNi_{1-y}Co_yO_2$ samples with y=0.2 and 0.4 can be seen in Fig. 7a,b, and that the b constant is related to the magnetic anisotropy, K, by the expression [20]

$$b = \beta\frac{K^2}{M_S^2}, \tag{10}$$

where β is a constant that depends on the type of material.

Assuming a typical value for the β constant (i.e., β=0.0762 [21]), we can deduce the magnetic anisotropy constant from first magnetization curves from

$$K = \left(\frac{bM_S^2}{0.0762}\right)^{1/2}. \tag{11}$$

Following this procedure, we find that the magnetic anisotropy value, which is 6.5×10^6 erg/cm^3 for the $LiNiO_2$ sample at 200 K, increases upon cobalt doping. Interestingly enough, these values are related to the volume of the magnetic clusters that lead to the blocking temperature in the $\chi_m(T)$ ZFC- and FC-type curves. In this context, we can assume [1]

$$KV = 25_{k_B}T_B, \tag{12}$$

where V is the volume of the magnetic clusters, k_B is the Boltzmann's constant, and T_B is the blocking temperature of each particular sample.

Now, supposing that these magnetic clusters are spherical, we obtain that they would have a mean radii of R=3.5 nm in the case of the $LiNiO_2$ sample, and that their size decreases upon Co-doping, becoming R=1.2 nm in the sample with y=0.2, and being further reduced to 0.5 nm in the samples with y=0.3 and 0.4, as shown in Fig. 7.

Magnetic properties of spinels

The spinel material $LiMn_2O_4$ can be cycled at ca. 4 V vs Li^+/Li from $LiMn_2O_4$ to λ-MnO_2 with manganese ions

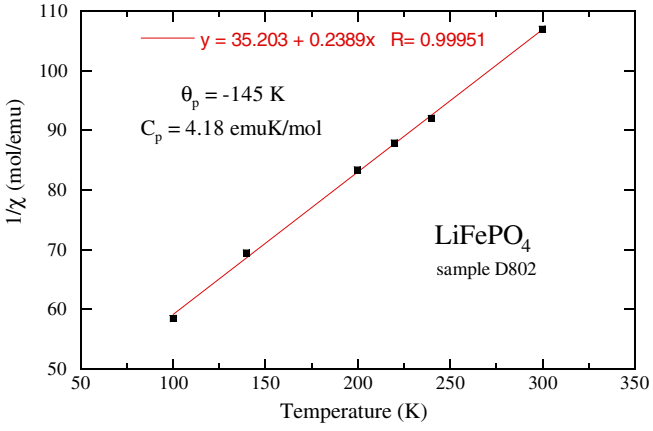

Fig. 13 Plot of the dM/dH slope of the magnetization curves to extract χ_m

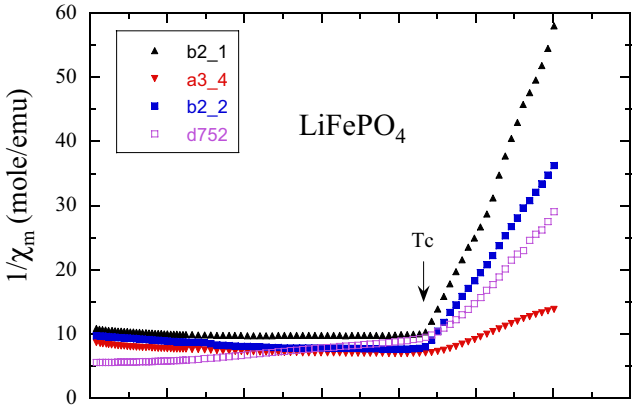

Fig. 14 The inverse of the magnetic susceptibility $\chi_m(T)$ of $LiFePO_4$ samples synthesized by different sol-gel methods

remaining the spinel host lattice throughout. $LiMn_2O_4$ spinel has shown interesting magnetic properties [22–27]. From the point of view of magnetic interactions, both direct ($Mn^{3+/4+}$–$Mn^{3+/4+}$) and superexchange (90° $Mn^{3+/4+}$–$O^{2-}$$Mn^{3+/4+}$) interactions are conceivable between the nearest Mn neighbors. According to Goodenough, only Mn^{4+}–$O^{2-}$$Mn^{4+}$ interaction is in ferromagnetic coupling, while all other interactions are in antiferromagnetic coupling [28].

λ-$Li_{0.08}MnO_2$

Figure 8 shows the inverse magnetic susceptibility obtained after the lithium extraction from $LiMn_2O_4$. Over the temperature range 100–300 K, assuming that only the spin part of the Mn ions contributes to paramagnetic moment, the fit of the Curie–Weiss law is obtained with the following values: θ_p=−75 K and C_p=3.29 emu K/mol. The θ_p value is negative, consistent with the apparent antiferromagnetic ordering below T_N=30 K. From the Curie constant, the effective moment is determined to be μ_{eff}=3.70μ_B, which is a value smaller than the theoretical spin-only value of 3.87μ_B for Mn^{4+} ion. An increase in the nominal manganese oxidation state from +3.5 to +4 should result in a greater covalence state due to the removal of σ antibonding e_g electrons associated with the manganese *3d* state. So, λ-MnO_2 has a greater covalency in the Li–O–Mn^{4+} bond than in the Li–O–$Mn^{3.5+}$ bond.

The abrupt increase of magnetization (insert of Fig. 8) is noticeable with decreasing temperature below 30 K, indicating the presence of a ferromagnetic component. The origin of this ferromagnet could be a small amount of impurity phases, such as ferromagnetic Mn_3O_4, which is probably produced during the lithium extraction from $LiMn_2O_4$. However, the observation of spin-glass behavior at temperatures below the paramagnetic regime in the cubic phases $LiMn_2O_4$ and λ-$Li_{0.07}MnO_2$ has been reported by Jang et al. [24]. The existence of frozen spins is consistent with the presence of a significant fraction of spins disordered well below the Néel temperature. The value of the ratio f=θ_p/T_N=2.5 is indicative of a frustrated antiferromagnet. The geometric frustration inherent in the Mn sublattice, which is comprised of a three-dimensional array of a corner-sharing tetrahedral, has been discussed by Greedan et al. [26].

$LiMn_2O_4$

Figure 9 shows the reciprocal magnetic susceptibility of a $LiMn_2O_4$ sample synthesized by wet-chemical technique, i.e., succinic-assisted sol-gel method [29]. In the temperature range 2–300 K, the ZFC and FC curves present complex behaviors including a Curie–Weiss law above 140 K. The extracted Curie–Weiss parameters are θ_p= −260 K and C_p=4.85 emu K/mol. The negative Weiss constant indicates that antiferromagnetic interactions are dominant over ferromagnetic superexchange interactions in the paramagnetic temperature regime. These are the exchange interaction components across a shared octahedral-site edge in $LiMn_2O_4$ [30].

The measured effective magnetic moment is μ_{eff}=4.29 μ_B. The value p_{eff}=4.29 is close to the theoretical spin-only value p_{eff}=4.38, assuming that only Mn^{3+} and Mn^{4+} moments are responsible to the paramagnetic behavior of $\chi_m(T)$, i.e., for $Mn^{3.5+}$ valence state (p_{eff}=3.87 and C_p=1.87 emu K/mol for Mn^{4+}; p_{eff}=4.90 and C_p=3.0 emu K/mol for Mn^{3+}). The magnetization curves display a clear splitting of the ZFC and FC data occurring below the paramagnetic temperature regime. A sharp maximum appears at 20 K in the ZFC magnetization. Jang et al. have reported a spin-glass-like behavior indicating the presence of frozen spins in cubic phases λ-MnO_2 and $LiMn_2O_4$ [31]. The randomness and frustration necessary for spin-glass-like behavior are explained by the octahedral antiferromagnetic network in the $[Mn_2]O_4$ sublattice spinel structure, combined with some magnetic disorder. The disorder due to the presence of a valence distribution in the Mn ions is provoked by competing ferro- and antiferromagnetic exchange interactions. This is believed to be responsible for the complex magnetic structure. Frozen spin was also observed in a neutron diffraction study by Oohara et al. [32]. Magnetic susceptibility measurements

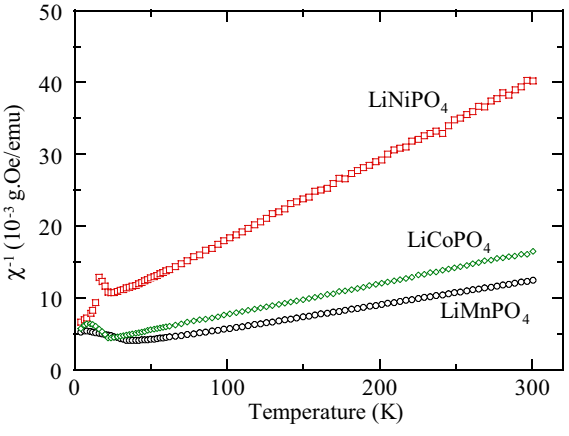

Fig. 15 The temperature dependence of the reciprocal magnetic susceptibility $\chi_m(T)$ of Li*M*PO_4 samples (*M*=Ni, Co, Mn)

Table 2 The Curie–Weiss constants and the effective magneton number for LiMPO$_4$

Compound	T_N (K)	θ_p (K)	C_p (emu K/mol)	p_{eff}
$LiMnPO_4$	38	−68	4.63	6.11
$LiNiPO_4$	24	−65	1.28	3.15
$LiCoPO_4$	22	−77	2.05	4.06
$LiFePO_4$	52	−145	4.18	5.77

were also made on oxygen-deficient spinel $LiMn_2O_{4-\delta}$ (δ=0–0.1) [33].

$LiMn_{2y}Co_yO_4$

Various substitutions of manganese by different transition-metal cations have been investigated to improve their electrochemical properties [29]. The Jahn–Teller distortion associated with a large change in cell volume that occurs in the discharged state of $LiMnO_4$ is avoided with an increasing average oxidation state of manganese ions, n_{Mn}>3.5+. On the basis of charge balance arguments, the substitution of a Mn ion for a dopant cation (e.g., Co, Cr, Ni, Al, Li, Zn, etc.) with charge n^+ will result in the oxidation of 2(3.5-n) Mn ions with average oxidation states of 3.5 to Mn^{4+}.

Figure 10 shows the temperature dependence of the magnetic susceptibility of $LiMn_{2-y}Co_yO_4$ ($0 \le y \le 1$) samples. In the low-temperature region, a drastic change in magnetization is observed upon substitution of Co for Mn. In particular, the strong anomaly at T=30 K disappears progressively with the introduction of Co^{3+} ions in the spinel lattice. This is a consequence of the disappearance of the Mn^{3+} ions in the $[Mn_2]O_4$ sublattice. For $LiCoMnO_4$, Mn^{4+} is the only paramagnetic species. For the y=1 sample, the curve $\chi(T)$ can be represented by a straight line obeying the Curie–Weiss law $\chi_m^{-1}=(T-\theta_p)/C_p$ in the entire temperature range (5–300 K). The very large negative Weiss temperature θ_p=−260 K for $LiMnO_4$ decreases to θ_p=−20 K for $LiMnCoO_4$, indicating a weaker antiferromagnetic interaction. Hence, it appears that Mn^{4+} ions in the [Mn^{4+} Co^{3+}] environment have a stable configuration at low temperature. This observation suggests that the cobalt ions themselves must impart a larger electron spin density through the metal–oxygen–lithium bond in addition to the increasing presence of Mn^{4+}.

Magnetic properties of Li-phosphates

Recently, transition metal-based compounds containing compact tetrahedral polyanion structural units have been investigated intensively as potential positive electrode materials for lithium-ion batteries [34–36]. They are considered as stable, nontoxic, and friendly environmental materials. These compounds can exhibit various voltage-composition dependencies originating from their different structures.

Phospho-olivine $LiFePO_4$

The $LiFePO_4$ olivine structure belongs to the orthorhombic *Pnma* space group. It consists of a distorted hexagonal close-packed framework containing Li and Fe in octahedral sites and P in tetrahedral sites. Each Li atom is connected by oxygen atoms to six FeO_6 units. The FeO_6 units are distorted, reducing the symmetry from O_h to C_s[2]. In C_s symmetry, the metal d-orbitals split into 3A' orbitals at higher energy than the two remaining A'' orbitals, unlike O_h symmetry, where two orbitals at higher energy are expected. The Fe magnetic ions are in the divalent Fe^{2+} state, and occupy only the M_2 site, i.e., the center of the FeO_6 octahedron unit, while Li occupies only the M_1 site. As a consequence, Fe is distributed so as to form FeO_6 octahedra isolated from each other in $TeOc_2$ layers perpendicular to the [001] hexagonal direction [37]. In addition, the lattice has a strong two-dimensional character because above a $TeOc_2$ layer comes a second layer, at the vertical of the previous one, to build (100) layers of FeO_6 octahedra sharing corners, and mixed layers of LiO_6 octahedra and PO_4 octahedra.

Figure 11 displays the reciprocal ZFC and FC magnetic susceptibility of $LiFePO_4$ measured at H=1 T. $LiFePO_4$ undergoes an antiferromagnetic transition at T_N=52 K, with

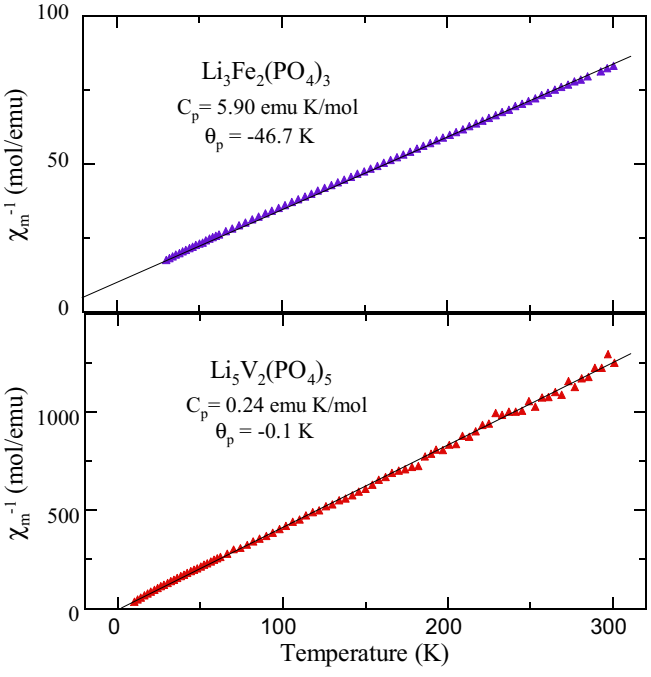

Fig. 16 The Curie–Weiss plots for **a** iron and **b** vanadium vitreous Nasicon-like materials

moments aligned along the [010] axis. The most outstanding property of the $\chi_m^{-1}(T)$ curve for $LiFePO_4$ lies in the fact that the deviation from the Curie–Weiss law remains small in the range 60–300 K. Values of Curie–Weiss constants deduced from the slope of the isothermal magnetization data (Fig. 11) are C_p=4.18 emu K/mol and θ_p=−145 K. These data are consistent with the magnetism of lithium iron phosphates where an antiferromagnetic ordering at low temperatures was reported [37]. The negative value of θ_p is consistent with the antiferromagnetic coupling known for this compound. The value of the effective moment μ_{eff}=5.77 μ_B is in agreement with what is expected for Fe(II) ions. The analysis of the exchange paths has been made by Mays [38].

Figure 12 displays the magnetization curves of $LiFePO_4$ in the temperature range 4–300 K. Due to the existence of a ferromagnetic component, the magnetization is not a linear function of the magnetic field. The first consequence is an ambiguity in what is called magnetic susceptibility χ_m, because M/H is distinct from dM/dH. Because all the magnetic measurements have been performed on a SQUID magnetometer (and not a Faraday balance), the quantity measured is the magnetization M in an applied magnetic field H, so that we shall use the notation $\chi_m=M/H$. The other consequence of the nonlinearity of the magnetization is that the data recorded in the "long-moment" made by the SQUID apparatus are not sufficient to get an understanding of the magnetic susceptibilities, and the full investigation of the magnetization as a function of the magnetic field at different temperatures is needed for this purpose (Fig. 13).

The inverse of the magnetic susceptibility $\chi_m(T)$ of $LiFePO_4$ samples synthesized by different sol-gel methods is reported as a function of temperature in Fig. 14. At contrast with prior works, these data give evidence of a ferromagnetic ordering at Curie temperature Tc~216 K, while we expected the evidence of an antiferromagnetic ordering at 52 K. Below Tc, the magnetic susceptibility is independent of temperature, and thus only depends on a demagnetization factor. Above Tc, the Curie–Weiss law is approximately satisfied with a Curie–Weiss temperature close to Tc. The effective Curie constant, however, is sample-dependent. In addition, the Curie–Weiss law is a mean-field law, and thus, valid only far from Tc. This condition, even at room temperature, is not fulfilled, which precludes any quantitative analysis of the magnetic susceptibility curves in Fig. 14 in this framework. Due to the existence of a large ferromagnetic component, the magnetization is not a linear function of the magnetic field [39].

$LiMPO_4$ olivine-related compounds

Other olivine structures $LiMPO_4$ include compounds with M=Ni, Co, and Mn. The temperature dependence of the inverse magnetic susceptibility measured with a SQUID magnetometer is shown in Fig. 15. All compounds exhibit a Curie–Weiss-type dependence on temperature. The data are consistent with the magnetism of $LiFePO_4$, where antiferromagnetic ordering appears at low temperatures. Linear fits provided the Weiss constants and the effective magnetic moments (Table 2), which can be compared to the theoretical spin-only values in Table 1. The reduced MO_6 symmetry has a noticeable effect on the magnetic susceptibility of $LiCoPO_4$. We note that Co^{2+} is expected to have three unpaired electrons (A') in C_s symmetry, consistent with the experimental data, but only a single unpaired electron (e_g) in O_h symmetry [40].

The magnetic structures in the ordered phases are both collinear for olivines: in $LiMnPO_4$ the magnetic moments are parallel to the a-axis, while in $LiFePO_4$ and $LiCoPO_4$, to the b-axis. In this case, the orbital angular momentum is not completely quenched, and spin-orbit coupling aligns spins along the b-axis. The distance between magnetic ions is one of the strongest factors affecting the magnetic exchange strength. This distance variation accounts well for the observed transition temperature: The highest T_N corresponds to the strongest exchange.

For the $LiFePO_4$ phospho-olivine structure, the magnetic properties give evidence of nano-sized ferromagnetic particles, which can be either strongly magnetic (γ-Fe_2O_3 clusters) or weakly ferromagnetic (Fe_2P clusters), depending on the preparation process. The concentration of magnetic clusters also depends on the preparation process and varies from small concentrations (1.0×10^{-6} of γ-Fe_2O_3 per formula), in which case, noncollective behavior is observed, to large concentrations (1.9×10^{-4} of Fe_2P clusters per formula) where the dipolar interaction generates superferromagnetism. Ferromagnetic resonance experiments are also reported and are a probe of the γ-Fe_2O_3 nanoparticles. An overall understanding of the different properties is achieved within a model of superferromagnetism induced by interacting Fe_2P nanoparticles (Ait Salah et al., unpublished).

$Li_xM_2(PO_4)_x$ compounds

Among the lithium metal polyphosphate family, the compounds described by formula $Li_xM_2(PO_4)_x$ (M=Fe, V, Mo and x=3, 5, 6, respectively) crystallize with the Nasicon-like structure [41]. Plots of the magnetic susceptibility, as a function of temperature for Fe- and V-containing compounds, are shown in Fig. 16. The calculated Curie temperature value equals θ=−46.7 K for $Li_3Fe_2(PO_4)_3$ and θ_p=−0.1 K for $Li_5V_2(PO_4)_5$. The negative Curie temperature indicates an antiferromagnetic behavior of the studied materials at temperatures above their Néel point. For $Li_3Fe_2(PO_4)_3$, the magnetic moment $\mu_{eff}\approx5.90\mu_B$ is comparable with the theoretical value of Fe^{3+} (5.92 μ_B). For the $Li_5V_2(PO_4)_5$ sample, one obtains $\mu_{eff}\approx1.56$ μ_B, while the theoretical value equals 1.55 μ_B for V^{4+} and 1.63 μ_B for V^{3+}. Values of the magnetic moment for both studied materials are associated with the most occupied transition metal sites [Fe^{3+} for $Li_3Fe_2(PO_4)_3$ and V^{4+} for $Li_5V_2(PO_4)_5$, respectively]. For the Mo compounds, a different behavior is observed. This material behaves as a diamagnetic material (i.e., its susceptibility is

negative and temperature-independent) in the whole range of temperature.

Conclusion

For $LiNi_{1-y}Co_yO_2$ materials prepared by wet chemistry, the magnetic measurements of $\chi_m(T)$ and $M(H)$ have revealed the presence of small ferromagnetic islands arising from the fact that some Ni^{2+} ions are occupying Li^+ places, which leads to a ferromagnetic ordering of the Ni ions in two adjacent $(Ni,CoO_2)_n$ slabs. The size of these clusters gets smaller and smaller as the Co content increases from $R_{(y=0)}$=3.5 nm to $R_{(y=0.4)}$=0.5 nm.

Magnetic characterization of $LiMn_2O_4$ spinel materials shows a spin-glass behavior below the paramagnetic regime (T_N<25 K). The magnetic properties are determined by interactions between the Mn ions, which in turn depend on the Mn valence distribution in the $[Mn_2]O_4$ framework. The short-range antiferromagnetic order is also investigated in the case of cobalt-substituted spinels, namely, $LiMn_{2y}Co_yO_4$.

For $LiFePO_4$ phospho-olivine material, the magnetic properties give evidence of nano-sized ferromagnetic particles, which can be either strongly magnetic (γ-Fe_2O_3 clusters) or weakly ferromagnetic (Fe_2P clusters), depending on the preparation process. The concentration of magnetic clusters also depends on the preparation process and varies from small concentration (1.0×10^{-6} of γ-Fe_2O_3 per formula), in which case, noncollective behavior is observed, to large concentrations (1.9×10^{-4} of Fe_2P clusters per formula) where the dipolar interaction generates superferromagnetism. Ferromagnetic resonance experiments are also reported and are a probe of the γ-Fe_2O_3 nanoparticles. An overall understanding of the different properties is achieved within a model of superferromagnetism, which is induced by interacting Fe_2P nanoparticles. The magnetic structure of $LiMPO_4$ phospho-olivine lattices is just that which is predicted by the application of Anderson's theory of superexchange to *M*–O–P–O–*M* linkages.

Acknowledgements We would like to thank Dr. N. Amdouni for providing the samples used in this work. Mr. M. Selmane is gratefully acknowledged for his assistance in XRD measurements. A. Ait-Salah's work is supported by a Ph.D. grant from the Morocco–French cooperation program under contract No. MA/03/71.

References

1. Morrish AH (2001) The physical principles of magnetism. IEEE, New York
2. Rodriguez-Carjaval J (1993) Physica B 192:55
3. Hibbs AD, Sager RE, Kumar S, McArthur JE, Singsaas AL, Jensen KG, Steindorf MA, Aukerman TA, Schneider HM (1994) Rev Sci Instrum 65:2544
4. Kittel C (1956) Introduction to solid state physics, 2nd edn. Wiley, New York
5. Ashcroft NW, Mermin ND (1976) Solid State Physics. Saunders College, New York
6. Ichida T, Shinjo T, Bando Y, Takada T (1970) J Phys Soc Jpn 29:79
7. Shirane T, Kanno R, Kawamoto Y, Takeda Y, Takano M, Kamiyama T, Izumi F (1995) Solid State Ionics 79:227
8. Tabuchi M, Tsutsui S, Masquelier C, Kanno R, Ado K, Matsubara I, Nasu S, Kageyama H (1998) J Solid State Chem 140:159
9. Hirakawa K, Kadowaki H, Ubukoshi K (1985) J Phys Soc Jpn 54:3526
10. Hirakawa K, Kadowaki H (1986) Physica B 136:335
11. Klemp JP, Cox PA, Hodby JW (1990) J Phys Condens Matter 2:6699
12. Hirota K, Nakazawa Y, Ishikawa M (1990) J Magn Magn Mater 90–91:279
13. Reimers JN, Dahn JR, Greedan JE, Stager CV, Liu G, Davidson I, von Sacken U (1993) J Solid State Chem 102:542
14. Yamaura K, Takano M (1996) J Solid State Chem 127:109
15. Shirakami T, Takematsu M, Hirano A, Kanno R, Yamaura K, Takano M, Atake T (1998) Mater Sci Eng B 54:70
16. Chappel E, Nunez-Regueiro MD, De Brion S, Chouteau G, Bianchi V, Courant D, Baffier N (2002) Phys Rev B 66:132412
17. Senaris-Rodriguez MA, Castro-Garcia S, Castro-Couceiro A, Julien C, Hueso LE, Rivas J (2003) Nanotechnology 14:277
18. Barra AL, Chouteau G, Stepanov A, Rougier A, Delmas C (1999) Eur Phys B 7:551
19. Saadoune I, Delmas C (1996) J Mater Chem 6:193
20. Holstein T, Primakoff H (1941) Phys Rev 59:388
21. Balcells L, Fontcuberta J, Martínez B, Obradors X (1998) Phys Rev B 58:14697
22. Sugiyama J, Hioki T, Noda S, Konani M (1998) Mater Sci Eng B 54:73
23. Jang Y, Chou FC, Chiang Y-M (1999) Appl Phys Lett 74:2504
24. Jang Y, Chou FC, Huang B, Sadoway DR, Chiang Y-M (2003) J Phys Chem Solids 64:2525
25. Arillo MA, Cuello G, Lopez ML, Martin P, Pico C, Veiga ML (2005) Solid State Sci 7:25
26. Greedan JE, Raju NP, Wills AS, Morin C, Shaw SM (1998) Chem Mater 10:3058
27. Wills AS, Raju NP, Morin C, Greedan E (1999) Chem Mater 11:1936
28. Goodenough JB (1963) Magnetism and the chemical bond. Wiley, New York
29. Julien C, Ziolkiewicz S, Lemal M, Massot M (2001) J Mater Chem 11:1837
30. Goodenough JB, Manthiram A, James ACWP, Strobel P (1989) Mater Res Soc Symp Proc 135:391
31. Jang Y, Chou FC, Huang B, Sadoway DR, Chiang Y-M (2000) J Appl Phys 87:7382
32. Oohara Y, Sugiyama J, Kontani M (1999) J Phys Soc Jpn 68:242
33. Sugiyama J, Atsumi T, Koiwai A, Sasaki T, Hioki T, Noda S, Kamegashira N (1997) J Phys Condens Matter 9:1729
34. Manthiram A, Goodenough JB (1987) J Solid State Chem 71:349
35. Padhi AK, Nanjundaswamy KS, Goodenough JB (1997) J Electrochem Soc 144:1188
36. Bykov AB, Chirkin AP, Demyanets LN, Doronin SN, Genkina EA, Ivanov-Shits AK, Kondratyuk IP, Maksimov BA, Melnikov OK, Muradyan LN, Simonov VI, Timofeeva VA (1990) Solid State Ionics 38:31
37. Santoro RP, Newnham RE (1967) Acta Crystallogr 22:344
38. Mays JM (1963) Phys Rev 131:38
39. Ait-Salah A, Zaghib K, Mauger A, Gendron F, Julien CM (2006) Phys Status Solidi (a) 203:R1
40. Tucker MC, Doeff MM, Richardson TJ, Finones R, Cairns EJ, Reimer JA (2002) J Am Chem Soc 124:3832
41. Morgan D, Ceder G, Saidi MY, Barker J, Swoyer J, Huang H, Adamson G (2002) Chem Mater 14:4684